

Quantum tops at the LHC: from entanglement to Bell inequalities

Claudio Severi^{a,1}, Cristian Degli Esposti Boschi^{b,3,4},
 Fabio Maltoni^{c,2,4,5}, Maximiliano Sioli^{d,2,4}

¹Department of Physics and Astronomy, University of Manchester, Manchester, United Kingdom

²Dipartimento di Fisica e Astronomia, Università di Bologna, via Irnerio 46, Bologna, Italy

³CNR-IMM, Sezione di Bologna, via Gobetti 101, 40129, Bologna, Italy

⁴INFN, Sezione di Bologna, via Irnerio 46, Bologna, Italy

⁵Centre for Cosmology, Particle Physics and Phenomenology, Université catholique de Louvain, Louvain-la-Neuve, Belgium

Abstract We present the prospects of detecting quantum entanglement and the violation of Bell inequalities in $t\bar{t}$ events at the LHC. We first introduce suitable observables and then perform an analysis using simulated events in the dilepton final state, up to the unfolded level. We find that entanglement can be easily established at better than 5σ both at threshold as well as at high- p_T already in the LHC Run 2 dataset. On the other hand, only very high- p_T events are sensitive to a violation of Bell inequalities, making it significantly harder to observe experimentally, even at the end of the LHC High Luminosity Run.

1 Introduction

Quantum Mechanics (QM) predicts that when an entangled pair of particles is created, the two-particle wavefunction retains a non-separable character when they are set apart. In particular, correlations on experimental measurements arise even when the observations are space-like separated. Were QM the emergent explanation of an underlying classical theory, the causal structure imposed by relativity would be violated. The issue can also be solved by postulating QM is incomplete, and additional *hidden* degrees of freedom exist. Ultimately, whether or not reality is described by QM is matter of experiment. In 1964, Bell proved [1] classical theories obey correlation limits, *i.e.*, Bell Inequalities (BIs), that QM can violate. In the last decades, several experiments have been performed and all results so far agree with QM predictions. Recently, prospects of using hadron colliders to test BIs at unprecedented scales of order of a TeV have emerged [2–4]. In this Letter, we explore the perspectives of experimentally observing entanglement as well as the violation of

^ae-mail: claudio.severi@postgrad.manchester.ac.uk

^be-mail: degliesposti@bo.imm.cnr.it

^ce-mail: fabio.maltoni@unibo.it

^de-mail: maximiliano.sioli@unibo.it

BIs using spin correlations in $t\bar{t}$ pairs produced in proton-proton collisions at the LHC, as first suggested in [2] and [3], respectively. By performing physics and (fast) detector simulations, we identify key observables that are sensitive to quantum effects, provide a method to measure them without introducing biases and estimate the prospects of observing entanglement and the violation of BIs at the present and future LHC runs.

2 Entanglement and Bell inequalities

The state of a system composed of two subsystems A and B is *separable* if its density matrix ρ can be written as:

$$\rho = \sum_{k=1}^n p_k \rho_A^k \otimes \rho_B^k, \quad (1)$$

where ρ_A^k and ρ_B^k are quantum states for A and B , and the coefficients p_k are non-negative and add to one. The density matrix (1) represents a system with *classical* probability p_k of being in the state $\rho_A^k \otimes \rho_B^k$. The state is *entangled* when it is not separable. Entanglement is a property of a system described in the framework of QM. A different question is whether measurements on a given system can violate BIs. These can be conveniently phrased in terms of Clauser, Horne, Shimony, and Holt (CHSH) inequality [5] which states that measurements a, a' and b, b' on subsystems A and B , respectively (with absolute value ≤ 1) *classically* must satisfy:

$$|\langle ab \rangle - \langle ab' \rangle + \langle a'b \rangle + \langle a'b' \rangle| \leq 2. \quad (2)$$

A particularly simple example is provided by two particles with non-zero spin. In this case, the measurements entering the CHSH inequality are their spin projections along four axes, \hat{a}, \hat{a}' for particle A , and \hat{b}, \hat{b}' for particle B . This corresponds to the situation which we will be considering in the following.

In QM, entanglement is a necessary condition for violating BIs. However, it is important to stress that in general, *i.e.*, for mixed states, the opposite is not true:

$$\text{Entanglement} \not\Rightarrow \text{Violation of BIs} . \quad (3)$$

A well-known example of states which can be entangled and yet not violate BI's are the so-called bipartite Werner states [6]. Let us consider a two spin- $\frac{1}{2}$ particle system, whose state is described by the simple density matrix:

$$\rho = \frac{1}{4} (\mathbb{1} \otimes \mathbb{1} + \sum_{i=1}^3 C_{ii} \sigma_i \otimes \sigma_i) , \quad |C_{ii}| < 1 . \quad (4)$$

This state gives already a (very good) approximation of the pattern of spin correlations in a $t\bar{t}$ system at the LHC and displays the features that will be important later.

The specific case where $C_{xx} = C_{yy} = C_{zz} = -\eta$ with $0 < \eta < 1$ corresponds to the singlet Werner state, while $C_{xx} = C_{yy} = -C_{zz} = \eta$ and cyclic permutations correspond to a triplet of Werner states (with fidelity $F = \frac{3\eta+1}{4}$). It is known that for Werner states, $\eta > 1/3$ implies entanglement, while the CHSH inequality is violated when $\eta > \sqrt{2}/2$.¹

More in general, one can identify the regions where the state (4) is entangled, using a criterion such as the one proposed in [7]. Independently, one can test whether directions $\hat{a}, \hat{a}', \hat{b}, \hat{b}'$ exist such that the CHSH inequality (2) is violated, using the theorem proven in [8]. The corresponding disjoint regions are depicted in Figure 1. Entanglement is present in the four light-colored small tetrahedrons which are inscribed in a large tetrahedron, while the CHSH inequality is violated only in the dark-colored sub-regions of the small tetrahedrons. The vertices of the large tetrahedron correspond to pure singlet and triplet Bell states, which we also use to identify the corresponding small tetrahedrons. The closer the C_{ii} 's are to vertices of the large tetrahedron the larger amount of spin correlations is present.

3 Top quark pairs at the LHC

Top quarks are unique candidates for high energy Bell tests. This follows from three concurring facts. First, $m_t \Lambda_{\text{QCD}}^{-2} \gg I_t^{-1}$, so top quarks decay semi-weakly before their spin is randomised by chromomagnetic radiation. Second, the leading top quark production mechanism at hadron colliders involves $t\bar{t}$ pairs where top quarks are not polarised yet their spins are highly (and not-trivially) correlated in different areas of phase space. Third, thanks to left-handed nature of the weak interactions, the charged lepton emerging from the

¹Werner states are usually expressed as mixtures of Bell states, $|\Phi^\pm\rangle$ and $|\Psi^\pm\rangle$. In particular, singlet and triplet Werner state correspond to one-parameter families of states that in the high-fidelity limit $F \rightarrow 1$ match pure singlet $|\Psi^-\rangle$ or (one of the three) triplet states $|\Psi^+\rangle, |\Phi^-\rangle, |\Phi^+\rangle$, respectively.

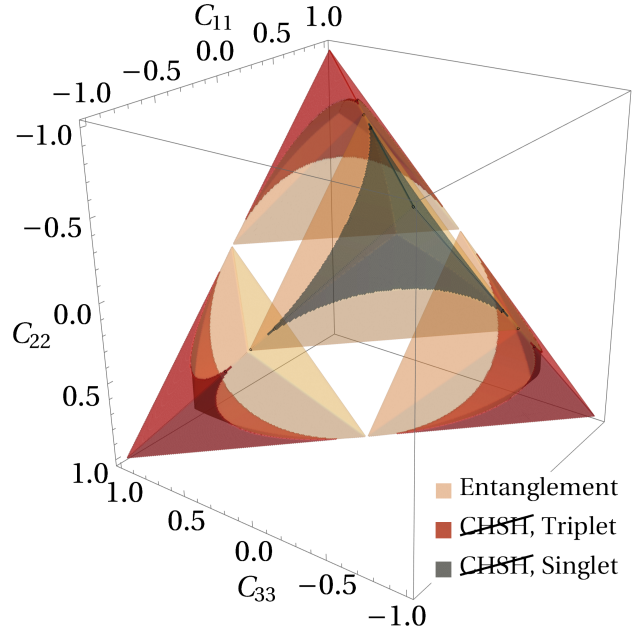


Fig. 1: Regions of $\{C_{11}, C_{22}, C_{33}\}$ phase space where the density matrix ρ in (4) is entangled, and where the CHSH inequality is violated, divided into triplet and singlet. Regions where ρ is not positive definite are not shown.

two-step decay $t \rightarrow Wb$ and $W \rightarrow \ell\nu$ turns out to be 100% correlated with the spin of the mother top quark, *i.e.* the top quark differential width is given by:

$$\frac{1}{\Gamma} \frac{d\Gamma}{d \cos \varphi} = \frac{1 + \alpha \cos \varphi}{2} , \quad (5)$$

with the spin analyzing power α attaining the largest possible values, *i.e.*, ± 1 . We denote φ the angle between the top spin and the direction of the emitted lepton in the top quark rest frame, see Figure 2. As a result, the lepton can be considered as a proxy for the spin of the corresponding top quark and the correlations between the leptons as a proxy for those between the top quark spins. Assuming no net polarisation is present², the density matrix for the spin of a $t\bar{t}$ pair can be written as:

$$\rho = \frac{1}{4} (\mathbb{1} \otimes \mathbb{1} + \sum_{i,j=1}^3 C_{ij} \sigma_i \otimes \sigma_j) . \quad (6)$$

where the first term in the tensor product refers to the top and the second term to the anti-top quark. The C_{ij} matrix en-

²Strong $t\bar{t}$ production does not lead to polarised top quarks, as parity is conserved [9]. EW effects (and possibly also absorptive parts from loops), on the other hand, can give rise to a net top quark polarisation. However, they have been estimated to be very small [10], and therefore are neglected here.

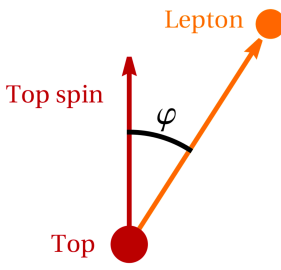


Fig. 2: Schematic representation of the decay of a top quark that ultimately leads to the emission of a charged lepton, in the top rest frame.

codes spin correlations, and it is measurable.³ The differential cross section for $pp \rightarrow t\bar{t} \rightarrow \ell^+ \ell^- b\bar{b} \nu \bar{\nu}$ can be expressed as [11]:

$$\frac{1}{\sigma} \frac{d\sigma}{dx_{ij}} = \frac{C_{ij} x_{ij} - 1}{2} \log |x_{ij}|, \quad (7)$$

where $x_{ij} \equiv \cos \theta_i \cos \bar{\theta}_j$, θ_i is the angle between the antilepton momentum and the i -th axis in its parent top rest frame, and $\bar{\theta}_j$ the angle between the lepton momentum and the j -th axis in its parent anti-top rest frame.⁴ Spin is measured fixing a suitable reference frame. An advantageous choice is the *helicity basis* $\{\hat{k}, \hat{r}, \hat{n}\}$,

$$\begin{cases} \hat{k} = \text{top direction} \\ \hat{r} = \frac{\hat{p} - \hat{k} \cos \theta}{\sin \theta} \\ \hat{n} = \hat{k} \times \hat{r}, \end{cases} \quad (8)$$

where \hat{p} is the beam axis and θ is the top scattering angle in the center of mass frame, see also Figure 3. The helicity basis is defined in terms of the top quark and also applies to the anti-top, which moves in direction $-\hat{k}$.

The amount and type of spin correlations strongly depend on the production mechanism as well as the phase space region (energy and angle) of the top quarks. Two complementary regimes are important: at threshold, *i.e.*, when the top quarks are slow in their rest frame, and when they are ultra-relativistic. At threshold, gluon fusion $gg \rightarrow t\bar{t}$ leads to an entangled spin-0 state while $q\bar{q} \rightarrow t\bar{t}$ to a spin-1 state. The latter is subdominant at the LHC and acts as an irreducible background [2].

It can be shown [7] that the $t\bar{t}$ spin density matrix (6) is separable (that is, not entangled) if and only if the partial

³Since $C_{ij} \approx C_{ji}$, the C matrix can be made (almost) diagonal with an appropriate choice of basis, thus reducing the system to the simple density matrix (4).

⁴Relevant reference frames are identified in a two step process: boosting first to the $t\bar{t}$ center of mass frame, then to each top with a rotation free boost.

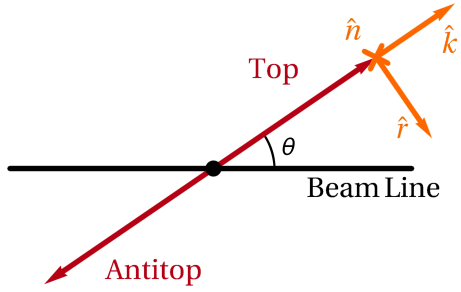


Fig. 3: Schematic representation of a $pp \rightarrow t\bar{t}$ event in the center of mass frame, with the helicity basis $\{\hat{k}, \hat{r}, \hat{n}\}$ drawn, together with the scattering angle θ . The \hat{n} axis is into the page.

transpose $(\mathbb{1} \otimes T)\rho$, obtained by acting with the identity on the first term of the tensor product and transposing the second, is positive definite. As shown in [2], this implies that

$$|C_{11} + C_{22}| - C_{33} > 1 \quad (9)$$

is a sufficient condition for the presence of entanglement. It generalises the Werner condition $\eta > 1/3$ to the case where the C_{ii} 's are not equal. The inequality (9) does not depend on the basis, but we will use the helicity basis (8) in the following.

At $t\bar{t}$ production threshold $C_{kk} + C_{rr} < 0$, so inequality (9) reads:

$$-C_{kk} - C_{rr} - C_{nn} > 1. \quad (10)$$

The second regime corresponds to high transverse momentum top quarks, *i.e.* when the system is characterised by $m_{t\bar{t}} \gg m_t$ and CMF scattering angle $\theta \sim \frac{\pi}{2}$. In this case, an entangled spin-1 state is produced as a consequence of conservation of angular momentum regardless of production channel. Since in this region $C_{kk} + C_{rr} > 0$, inequality (9) is written as:

$$C_{kk} + C_{rr} - C_{nn} > 1. \quad (11)$$

As for BIs, as shown in [8, 12] the maximal deviation predicted by QM in the CHSH inequality (2) is:

$$\max_{aa'bb'} |\langle ab \rangle - \langle ab' \rangle + \langle a'b \rangle + \langle a'b' \rangle| = 2\sqrt{\lambda + \lambda'}, \quad (12)$$

where λ and λ' are the two largest eigenvalues of $C^T C$. In [3] it was argued that requiring $\lambda + \lambda' > 1$ provides an easy way to test the CHSH violation. Unfortunately, we find that the method suggested in [3] entails a rather serious bias. Estimating the eigenvalues of random matrices is a notoriously hard problem [13]. Random fluctuations are more likely to

drive the eigenvalues of $C^T C$, which are necessarily greater than zero, in the positive direction rather than in the negative one. Furthermore, when selecting the two largest eigenvalues λ and λ' one is more likely to pick the ones that fluctuated up rather than those that fluctuated down. As a result, the estimated value of $\lambda + \lambda'$ is on average larger than the true value. To avoid these effects, we prefer to a-priori choose directions $\hat{a}, \hat{a}', \hat{b}, \hat{b}'$ (based on physical arguments), and then measuring spin correlations directly from the differential distributions. In so doing, we do not find any significant bias.

Spin correlations at threshold are strong enough to show entanglement but not enough to allow the observation of a violation of BIs. In addition, as we will discuss in the following, top quarks are moving slowly and their decays are usually not causally disconnected. On the other hand, a violation of BIs is expected at large $m_{t\bar{t}}$ and θ . A spin correlation experiment in this regime is equivalent to the usual quantum optics experiment with entangled photons, for which the optimal choice of axes is known to be:

$$\begin{aligned} a &= (0, 1, 0), \quad a' = (0, 0, 1), \\ b &= (0, -\frac{1}{\sqrt{2}}, \frac{1}{\sqrt{2}}), \quad b' = (0, \frac{1}{\sqrt{2}}, \frac{1}{\sqrt{2}}), \end{aligned} \quad (13)$$

where vectors are expressed in the helicity basis.⁵ Adopting the axes in Eq.(13), the CHSH inequality (2) can then be cast in a particularly simple form:

$$\sqrt{2} | -C_{rr} + C_{nn} | \leq 2, \quad (14)$$

which, once again, generalises the CHSH condition derived for Werner states. Note the \hat{k} axis does not appear in (14), consistent with the physical argument that in a Bell experiment the spin (helicity) of a massless particle is measured on a plane perpendicular to its motion. This test shows a striking similarity with the usual experiments in quantum optics used to probe a violation of BIs with two entangled photons, except for being characterised by a 10^{12} times larger energy.

4 Simulation and analysis

We generate events corresponding to proton–proton collisions at $\sqrt{s} = 13$ TeV resulting in a $\ell^- \ell^+ v \bar{v} b \bar{b}$ final state. Leptons ℓ only include electrons and muons, both in same and different flavor combinations. Non–resonant, single resonant and double resonant top quark diagrams are summed, as well as diagrams in which no top quarks exist, yet the

⁵An optimal choice of axes exists for every bin of $m_{t\bar{t}}$ and θ through which correlations are maximised [14]. We have checked that such an "event-by-event" choice, which reproduces (13) at large $m_{t\bar{t}}$ and θ , does not significantly extend the region in phase space where the CHSH inequality is violated. For simplicity (and to avoid possible biases), we opt for choice of axes (13) for all events.

final state is two bottom quarks, two leptons, and two neutrinos. Events are generated using `MadGraph5_aMC@NLO` [15] at Leading Order (LO) within the SM. This amounts to ~ 5000 diagrams summed. No kinematic cuts are imposed except for a lower limit of 5 GeV on the invariant mass of same flavor lepton pairs, to keep the $\gamma^* \rightarrow \ell^+ \ell^-$ splitting infrared safe. The rate is normalised to an estimate of the experimental cross section of $pp \rightarrow \ell^- \ell^+ v \bar{v} b \bar{b}$ obtained with recent measurements [16]. Hard processes are showered and hadronised using `Pythia 8` [17]. Events are then passed to the `Delphes` framework [18] for fast detector and reconstruction simulation, using the setup of ATLAS detector at the LHC. In our simplified analysis, we only consider irreducible backgrounds, consisting of contributions to the $\ell^- \ell^+ v \bar{v} b \bar{b}$ final state without an intermediate $t\bar{t}$ pair, or with an intermediate $t\bar{t}$ pair that does not decay into prompt light leptons. These contributions become negligible when the kinematics of two on-shell top quarks is correctly reconstructed. Further sources of background include $t\bar{t}V$ events, diboson events, and misidentification of leptons. These backgrounds are known to amount to a few percent of the total [19] and are neglected. The same flavor channel also receives a contamination from $Z + \text{jets}$ events, whose number, after cuts, is at the percent level [20], comparable with other backgrounds already quoted. At the selection level, we require the presence of at least two jets with $p_T > 25$ GeV and $|\eta| < 2.5$. At least one jet has to be b -tagged. If only one jet has been b -tagged, we assume the second b -jet is the one not b -tagged with the largest p_T . We require exactly two leptons of opposite charge, both with $p_T > 25$ GeV and $|\eta| < 2.5$. Both leptons must pass an isolation requirement. In the $e^+ e^-$ and $\mu^+ \mu^-$ channels, $Z + \text{jets}$ processes are suppressed by requiring $p_T^{\text{miss}} > 40$ GeV and 20 GeV $< m_{\ell^+ \ell^-} < 76$ GeV or $m_{\ell^+ \ell^-} > 106$ GeV. Before reconstructing neutrinos, the measured momenta of b quarks and the value of the missing energy are smeared according to the simulated distribution of reconstructed values around true values. Neutrinos are then reconstructed solving for the kinematics of $t\bar{t} \rightarrow \ell^- \ell^+ v \bar{v} b \bar{b}$. The solution is assigned a weight proportional to the likelihood of producing a neutrino of the given reconstructed energy in a $pp \rightarrow t\bar{t} \rightarrow \ell^- \ell^+ v \bar{v} b \bar{b}$ at $\sqrt{s} = 13$ TeV in the SM. If many solutions exist for the kinematics, all solutions are assigned weights and considered. The smearing on b quarks and p_T^{miss} is repeated 100 times. There is a twofold ambiguity in assigning b quarks to jets, so reconstruction is performed twice for each event. The assignment yielding the largest sum of weights is chosen, and the final p_V and $p_{\bar{V}}$ are calculated as a weighted average. The reconstructed distributions of $\cos \theta_i \cos \bar{\theta}_j$ appearing in (7) are unfolded using the iterative Bayesian method [21] implemented in the `RooUnfold` framework [22]. Distributions are unfolded iteratively until

stable. Details on the performance of our event reconstruction algorithm can be found in [14].

In order to verify the robustness of our observable definition and reconstruction method against higher-order QCD effects, we have generated 250 fb^{-1} of $pp \rightarrow t\bar{t}$ events at $\sqrt{s} = 13\text{ TeV}$ at Next-to-Leading Order (NLO) in QCD with MadGraph5_aMC@NLO. Since NLO QCD corrections to the C_{ij} matrix are known to be small [9], top spin correlations and finite width effects have been taken into account using MadSpin [23]. The test statistics (10), (11), and (14) are then re-evaluated using the event reconstruction algorithm cited above. Deviations in our region of interest are seen at the percent level, meaning the algorithm is well-behaved under the introduction of NLO QCD corrections, and missing higher order terms in our LO analysis are sub-leading with respect to statistical uncertainty in realistic LHC scenarios.

5 Results

As a first step, we consider the observation of entanglement. The two signal regions of interest are i) at threshold and ii) at large p_T . We consider three different selections, characterised by different trade-offs between keeping the largest possible statistics and maximising the correlations. The three selections are shown explicitly in Figure 4. The rationale behind the choice of selections is the following: the weakest selection includes all regions of phase space where our Monte Carlo suggests the numerical value of (10) or (11) exceeds 1 at parton level. The second selection is more stringent and amounts to only including regions with an expected value larger than 1.1. The third selection is the strongest, and only considers regions with a numerical value larger than 1.2, again at parton-level. Results are collected in Table 1, together with an estimate of the cross section included in each selection. When considering the LHC Run 2 luminosity of 139 fb^{-1} , the statistical significance for the detection of entanglement is of order 5σ or more in both signal regions.

The strategy to observe a violation of BIs is the same as the one employed for entanglement. In this case, however, we only consider one signal region, corresponding to events with $m_{t\bar{t}}$ of order TeV and θ close to $\frac{\pi}{2}$. We consider three selections, shown explicitly in Figure 5. Again, the selection regions have been chosen based on Monte Carlo parton-level expectations, and correspond to regions of phase space where the value of (14) exceeds 2, 2.1 and 2.2 at parton-level, respectively. Table 2 collects the corresponding results. We find that LHC Run 2 + Run 3 statistics are not sufficient for a conclusive measure of the value of (14). In order to provide an estimate for the upcoming High-Luminosity Run (HL-LHC), we estimate statistical uncertainties running our analysis on 3 ab^{-1} of simulated luminosity. Results are

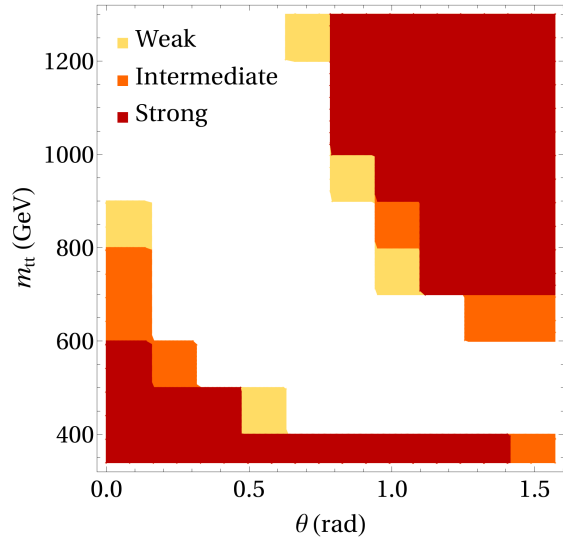


Fig. 4: Choice of cuts in $m_{t\bar{t}} - \theta$ space for the detection of entanglement.

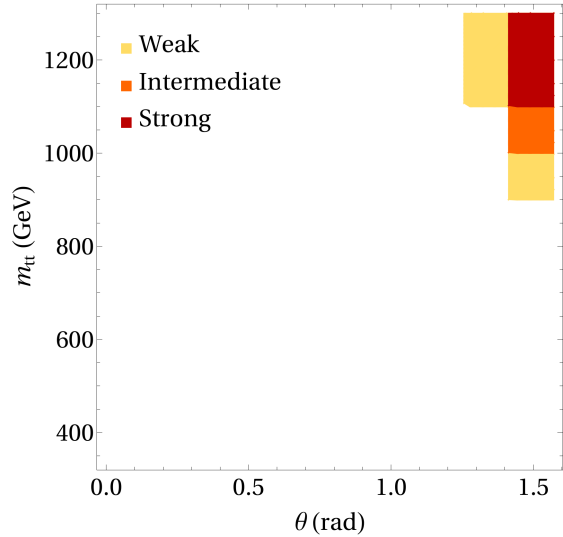


Fig. 5: Choice of cuts in $m_{t\bar{t}} - \theta$ space for the observation of a violation of the CHSH inequality.

collected in the fourth column of Table 14 and shown in Figure 6. The statistical significance for a violation of the CHSH inequality (14) becomes of order 1σ .

6 Loopholes

When performing a Bell experiment the possible existence of loopholes has to be assessed.

First, Bell experiments require outside intervention to choose *freely*, *i.e.* unknown to the system itself, what to measure. This can be achieved, for example, by mechanisms that randomly choose the orientations of the measurement axes.

Region	Selection	Cross section	$ C_{kk} + C_{rr} - C_{nn} $	
			Reconstructed	Significance for > 1
Threshold	Weak	14 pb	1.31 ± 0.02	$\gg 5\sigma$
	Intermediate	12 pb	1.34 ± 0.02	$\gg 5\sigma$
	Strong	10 pb	1.38 ± 0.02	$\gg 5\sigma$
High- p_T	Weak	1.9 pb	1.32 ± 0.07	5σ
	Intermediate	1.5 pb	1.36 ± 0.08	4σ
	Strong	1.0 pb	1.42 ± 0.13	3σ

Table 1: Results for the entanglement markers (11) and (10) in the two signal regions, for the selections explained in the text. For each selection an estimate of the cross section at 13 TeV is also reported. The quoted results are the average of several (5) independent simulated experiments using 139 fb^{-1} of luminosity (LHC Run 2) each. Values follow from the fit of (7), uncertainty is statistical only.

High- p_T Selection	Cross section	Parton-level	$\sqrt{2} C_{rr} + C_{nn} $		
			Reconstructed	Uncertainty w/ 350 fb^{-1}	Uncertainty w/ 3 ab^{-1}
Weak	80 fb	2.14	2.16	± 0.46	± 0.16
Intermediate	35 fb	2.22	2.23	± 0.84	± 0.27
Strong	21 fb	2.27	2.36	± 1.20	± 0.40

Table 2: Results for the left-hand side of the CHSH inequality (14) for different final state selections (details in the text). For each selection an estimate of the cross section at 13 TeV is reported. The quoted central values are the average of several (14) independent simulated experiments using 350 fb^{-1} of luminosity (LHC Run 2 + 3) each. Values follow from the fit of (7) and uncertainties are statistical only. In the last column we report the statistical uncertainties coming from the unfolding of 3 ab^{-1} of simulated luminosity (HL-LHC).

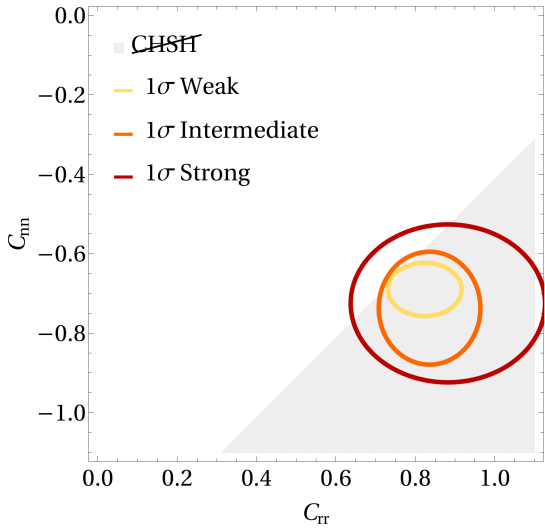


Fig. 6: Representation of results of Table 2 in the $C_{rr} - C_{nn}$ plane. Shaded band: region where CHSH inequality is violated. Ellipses: 1σ contour estimations for the value of C_{rr} and C_{nn} after the HL-LHC Run for the three selections. Stronger cuts move the central value further into the non-classical region, yet widen the uncertainties.

In the case of a $t\bar{t}$ system, no outside intervention is possible. However, one can argue that a random choice of axes is

realised by the direction of the final state leptons in the top quark decays.

Second, the quantum measurement of the spin state of the $t\bar{t}$ pair, which takes place when the top quarks decay leptonically, happens at very short distances. This is in contrast to the typical Bell experiment setups which feature macroscopic distances, and relate events that are always causally disconnected. In the case of the $t\bar{t}$ system, one can establish the causal independence of the decays only at the statistical level. In Figure 7 we plot a Monte Carlo evaluation of the probability of space-like separated decays as a function of the pair invariant mass $m_{t\bar{t}}$. Close to threshold, most of the top pairs decay within their light-cone, while more than 90% of $t\bar{t}$ pairs decay when they are space-like separated for $m_{t\bar{t}} > 800 \text{ GeV}$.

Third, even assuming b -tagging and lepton identification were perfect, one can only observe $pp \rightarrow \ell^- \ell^+ b\bar{b} + E^{\text{miss}}$. In fact, top quarks might even not be present in a given event. However, within our simulations, we have verified that after reconstruction the large majority of the events selected can be attributed to $t\bar{t}$ pair production.

Fourth, only a small fraction of events is usable for the analysis, and one has to assume the events that are recorded provide an unbiased representation of the bulk.

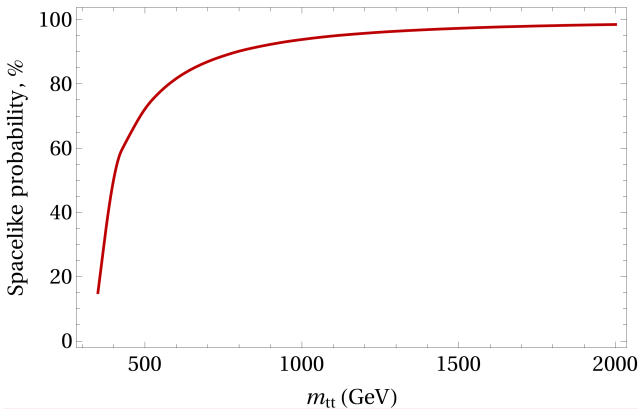


Fig. 7: Fraction of t and \bar{t} decays that are space-like separated as a function of $m_{t\bar{t}}$.

7 Conclusions

We have presented a feasibility study for the detection of entanglement and the violation of Bell inequalities using spin-correlation observables in top quark pairs at the LHC. The main motivation for such a measurement is the possibility of performing a first TeV-scale Bell experiment, opening new prospects for high-energy precision tests of QM. We have identified observables that are sensitive to either the presence of entanglement or to a violation of a CHSH inequality. Our results indicate that the detection of entanglement will be straightforward, and as already noted in [2], barring unexpected effects from systematic uncertainties, the LHC Run 2 dataset should be enough to reach a 5σ statistical significance. On the other hand, assessing the violation of Bell inequalities is much more challenging: sufficiently strong correlations are found only for top quarks at very high- p_T , thereby reducing the available statistics considerably. By considering only dileptonic final states and ignoring possibly relevant systematic uncertainties, whose evaluation goes beyond the scope of this study, we find the statistical significance for a violation to be of order 1σ at the end of the High-Luminosity Run. Barring the obvious benefits of an increased collider energy/luminosity, further studies to improve the prospects could be envisaged. For example, one could consider whether a likelihood ratio test with competing hypotheses would bring more discriminating power, or whether the limited statistics would be improved by including final states where only one top quark decays leptonically.

8 Acknowledgements

We are thankful to Eleni Vryonidou and Marco Zaro for comments on the manuscript and to Stefano Forte and Rikkert Frederix for discussions. F. M. has received funding from the European Union's Horizon 2020 research and innovation

programme as part of the Marie Skłodowska-Curie Innovative Training Network MCnetITN3 (grant agreement no. 722104) and by the F.R.S.-FNRS under the 'Excellence of Science' EOS be.h project n. 30820817.

References

1. J. S. Bell. On the Einstein Podolsky Rosen paradox. *Physics Physique Fizika*, 1(3):195–200, 1964. doi: 10.1103/PhysicsPhysiqueFizika.1.195.
2. Y. Afik and J.R.M. de Nova. Quantum information and entanglement with top quarks at the LHC. 2020. <http://arxiv.org/abs/2003.02280>.
3. M. Fabbrichesi, R. Floreanini, and G. Panizzo. Testing Bell inequalities at the LHC with top-quark pairs. 2021. <http://arxiv.org/abs/2102.11883>.
4. Y. Takubo et al. On the feasibility of bell inequality violation at atlas with flavor entanglement of b0-b0 pairs. 2021. <http://arxiv.org/abs/2106.07399>.
5. J.F. Clauser, Horne M.A., A. Shimony, and R.A. Holt. Proposed experiment to test local hidden-variable theories. *Physical Review Letters*, 23(15):880–884, 1969. doi: 10.1103/PhysRevLett.23.880.
6. Reinhard F. Werner. Quantum states with einstein-podolsky-rosen correlations admitting a hidden-variable model. *Physical Review A*, 40:4277, 1989. doi: 10.1103/PhysRevA.40.4277.
7. A. Peres. Separability criterion for density matrices. *Physical Review Letters*, 77, 1996. doi: 10.1103/PhysRevLett.77.1413. <http://arxiv.org/abs/quant-ph/9604005>.
8. R. Horodecki, P. Horodecki, and M. Horodecki. Violating Bell inequality by mixed spin- $\frac{1}{2}$ states: necessary and sufficient condition. *Physics Letters A*, 200, 1995. doi: 10.1016/0375-9601(95)00214-N.
9. W. Bernreuther, A. Brandenburg, Z. G. Si, and P. Uwer. Top quark spin correlations at hadron colliders: Predictions at next-to-leading order QCD. *Physical Review Letters*, 87:242002, 2001. doi: 10.1103/PhysRevLett.87.242002. <http://arxiv.org/abs/hep-ph/0107086>.
10. Rikkert Frederix, Ioannis Tsinikos, and Timea Vitos. Probing the spin correlations of $t\bar{t}$ production at NLO QCD+EW. *Eur. Phys. J. C*, 81(9):817, 2021. doi: 10.1140/epjc/s10052-021-09612-9.
11. W. Bernreuther, A. Brandenburg, Z.G. Si, and P. Uwer. Top quark pair production and decay at hadron colliders. *Nuclear Physics B*, 690(1-2):81–137, 2004. doi: 10.1016/j.nuclphysb.2004.04.019. <http://arxiv.org/abs/hep-ph/0403035>.
12. S. Chen, Y. Nakaguchi, and S. Komamiya. Testing Bell's inequality using charmonium decays. *Progress of Theoretical and Experimental Physics*, 2013(6), 2013.

doi: 10.1093/ptep/ptt032. <http://arxiv.org/abs/1302.6438>.

13. Z. Füredi and J. Komlos. The eigenvalues of random symmetric matrices. *Combinatorica*, 1, 1981.
14. C. Severi. Bell inequalities with top quark pairs with the ATLAS detector at the LHC. 2021. <http://amslaurea.unibo.it/23535/>.
15. J. Alwall et al. The automated computation of tree-level and next-to-leading order differential cross sections, and their matching to parton shower simulations. *Journal of High Energy Physics*, 79, 2014. doi: 10.1007/JHEP07(2014)079. <http://arxiv.org/abs/1405.0301>.
16. Particle Data Group. Review of particle physics. *Progress of Theoretical and Experimental Physics*, 2020(8), 2020. doi: 10.1093/ptep/ptaa104. <http://pdg.lbl.gov>.
17. T. Sjöstrand et al. An introduction to PYTHIA 8.2. *Computer Physics Communications*, 191, 2015. doi: 10.1016/j.cpc.2015.01.024. <http://arxiv.org/abs/1410.3012>.
18. DELPHES Collaboration. DELPHES 3: a modular framework for fast simulation of a generic collider experiment. *Journal of High Energy Physics*, 57, 2014. doi: 10.1007/JHEP02(2014)057. <http://arxiv.org/abs/1307.6346>.
19. ATLAS Collaboration. Probing the quantum interference between singly and doubly resonant top-quark production in pp collisions at $\sqrt{s} = 13$ TeV with the ATLAS detector. *Physical Review Letters*, 121, 2018. doi: 10.1103/PhysRevLett.121.152002. <http://arxiv.org/abs/1806.04667>.
20. CMS Collaboration. Measurement of the top quark polarization and $t\bar{t}$ spin correlations using dilepton final states in proton-proton collisions at $\sqrt{s} = 13$ TeV. *Physical Review D*, 100, 2019. doi: 10.1103/PhysRevD.100.072002. <http://arxiv.org/abs/1907.03729>.
21. G. D'Agostini. Improved iterative Bayesian unfolding. 2010. <http://arxiv.org/abs/1010.0632>.
22. T. Adye et al. Roounfold gitlab repository. 2021. <https://gitlab.cern.ch/RooUnfold/RooUnfold>.
23. P. Artoisenet et al. Automatic spin-entangled decays of heavy resonances in Monte Carlo simulations. *Journal of High Energy Physics*, 3, 2013. doi: 10.1007/JHEP03(2013)015. <http://arxiv.org/abs/1212.3460>.